Direct Measurement of the Bohr Magneton Using the Zeeman Effect and a Fabry-Pérot Etalon

Antoine Belley, Manuel Bolduc and Pierre-Alexis Roy

McGill University Department of Physics

Supervisors: Thomas Brunner and Dominic Ryan

February 2, 2020

Abstract

We use the Zeeman effect to measure the Bohr magneton using a Fabry-Pérot (FP) etalon. The FP apparatus was used to produce interference patterns in the 643.8 nm ray of light emitted by a cadmium lamp placed into a magnetic field. The magnetic field created in the middle of two electromagnets was calibrated using a Hall probe in order to get a correspondence between the voltage measured at a shunt resistor of 0.01 Ω across the power supply and the applied magnetic field. Pixel intensity analysis on images of the diffraction pattern taken with a CCD camera was then achieved on the circular interference patterns to obtain the distance between peaks of constructive interference. Using circular cross-correlation and multiple Gaussian least-square fits on the constructive interference peaks, the value of the Bohr magneton was measured to be of $7 \pm 6 \times 10^{-24} J/T$. This result is in agreement with the accepted value of $9.2740100783(28) \times 10^{-24} J/T$ [1].

Contents

1 Introduction **1**

2 Apparatus **2**

3 Magnetic Field Calibration **3**

3.1 Data analysis 3

3.2 Results and Error analysis 4

4 Fabry-Pérot Measurement **5**

4.1 Theory 5

4.2 Results 6

4.3 Data analysis 8

4.4 Validity 10

5 Conclusion **10**

6 Aknowledgments **10**

7 Appendix **12**

7.1 Error propagation for δ and Δ 12

1 Introduction

In quantum mechanics, the state of the particles are determined by the quantum numbers n, l and m_l, respectively representing the energy state, the angular momentum magnitude and angular momentum direction of the atom [2]. The angular momentum component of the atom's state induces a magnetic moment in the atom itself which interacts with a given exterior magnetic field B. This interaction will split the energy levels of the atom as a function of the magnetic quantum number m_l [2]. This is the effect known as the Zeeman effect. The energy levels splitting resulting from the Zeeman effect are described by

$$\Delta E \approx \frac{e\hbar}{2m_e c} B, \tag{1}$$

where e and m_e are the electronic charge and mass respectively, $\hbar$ is Planck's constant divided by 2π, c is the speed of light and B is the magnitude of the magnetic field [2]. In equation 1, the constants in front can be regrouped into one constant,

$$\mu_B = \frac{e\hbar}{2m_e c}, \tag{2}$$

known as the Bohr magneton [2], which has an accepted value of $9.2740100783(28) \times 10^{-24} J/T$ [1]. In this experiment, the goal is to use the Zeeman splitting to measure the Bohr magneton. A Cadmium lamp placed into a magnetic field emits light that will go through a Fabry-Pérot (FP) interferometer. This creates a diffraction pattern of concentric rings of constructive interference. As the magnitude of the magnetic field is increased, the atomic energy levels split in three due to the Zeeman interaction, such that quantum states with $m_l \in \{-1, 1\}$ will undergo a different observable splitting than the states with $m_l = 0$. This results in a splitting of diffraction rings into three rings (one for each m_l). These emitted rays of lights are polarized as a function of their quantum number m_l. Hence, using a polarizer allows us to study separately the $m_l = 0$ line and the $m_l = \pm 1$ lines [3].

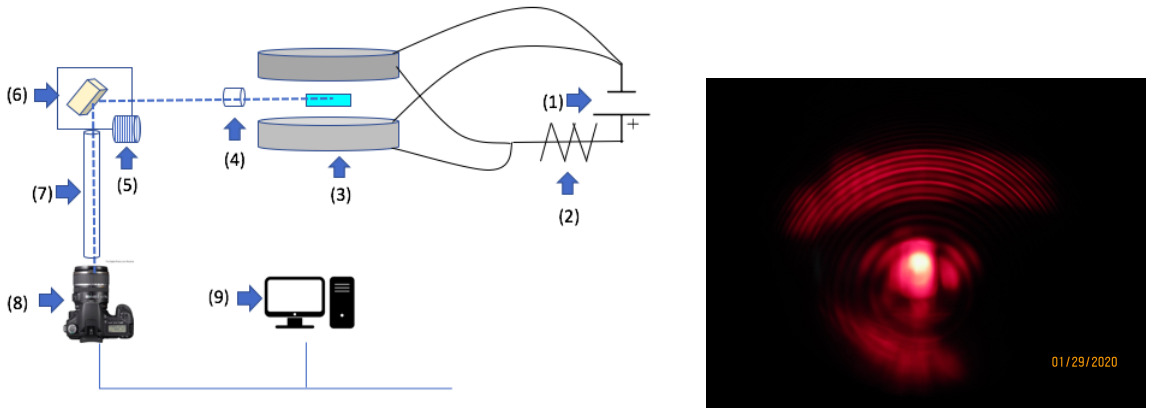

(a) (b)

Figure 1: **(a)** Schematics of the apparatus for the interferometer set up. The spectral tube is placed in the middle of the electromagnets (3), connected to the power supply (1). We measure the power supply current across the shunt resistor (2). The light emitted by the spectral tube (represented by the blue dashed line) is redirected by the constant deviation prism (6) (which can be rotated with the milled ring (5)) towards the camera (8), which is placed on a stand for proper adjustment. The observed spectrum can then be transferred to the computer (9) to perform pixel intensity analysis. The Fabry-Pérot Etalon(7) is placed in between the constant deviation prism and the camera. A rotating polarized filter is also placed before the deviation prism (4) to help distinguish the rays of light corresponding to different Zeeman splitting. **(b)** Interference pattern given by the Fabry-Pérot Etalon when observing the 643.8 nm spectral line of a cadmium lamp placed in a magnetic field of $0.62 \pm 0.06T$ without polarizer. On this picture, Zeeman splitting is apparent.

2 Apparatus

Figure 1a shows the basic set up for the Fabry-Pérot (FP) experiment. Calibration of the magnetic field in the middle of the electromagnets (3) is performed using a Hall probe. The FP Etalon (7) is then placed along the path of the light ray, after the constant deviation prism (6), which is adjusted so that the 643.8 nm red line emitted by the Cadmium lamp is directed into the FP Etalon and subsequently into the CCD camera (8). A red filter is placed just before the FP apparatus to isolate the red light in the recorded images. A polarizer (4) is placed before the constant deviation prism in order to isolate different rays of light resulting from the Zeeman splitting depending on its orientation. The CCD camera (8) is set at minimal shutter speed and maximal aperture so that the amount of light recorded by the camera is sufficient to get clear and detailed pictures.

The FP Etalon is adjusted such that the brightest point in the image (corresponding to the Cadmium light source) is placed in the centre of the image. Hence, this bright point does not mask the diffraction pattern in the rest of the image. Pictures are then taken at different values for the magnitude of the magnetic field and at different orientations of the polarizer.

Figure 1b shows an example of the circular diffraction pattern observed with this set up. As the magnetic field gets stronger, the diffraction rings split into three components because of the Zeeman effect and the radius of each ring is determined by the strength of the magnetic field.

3 Magnetic Field Calibration

In this experiment, the magnetic field created by the electromagnets is calibrated using a Hall probe for which the correspondence between the voltage in the Hall probe and the magnetic field perceived by the Hall probe is known [4]. To ensure the Hall probe is placed in the centre of the electromagnets, the probe is moved in the plane of the electromagnets until it maximizes the voltmeter reading of the Hall probe voltage and is then moved in the axial direction of the coils until the voltage across the probe is minimized.

3.1 Data analysis

Measurements of the voltage in the Hall probe are made for different values of the voltage across the shunt resistor on the power source. This allows the use of a linear interpolation in order to associate the voltage across the shunt resistor of 0.01 Ω to the magnetic field between the electromagnets. Then, a third order polynomial [5] least-square fit is performed on the values of the magnetic field as a function of the voltage across the shunt resistor. As shown in figure 2, the dependence is linear at lower values of the power supply voltage and flattens out at higher voltages.

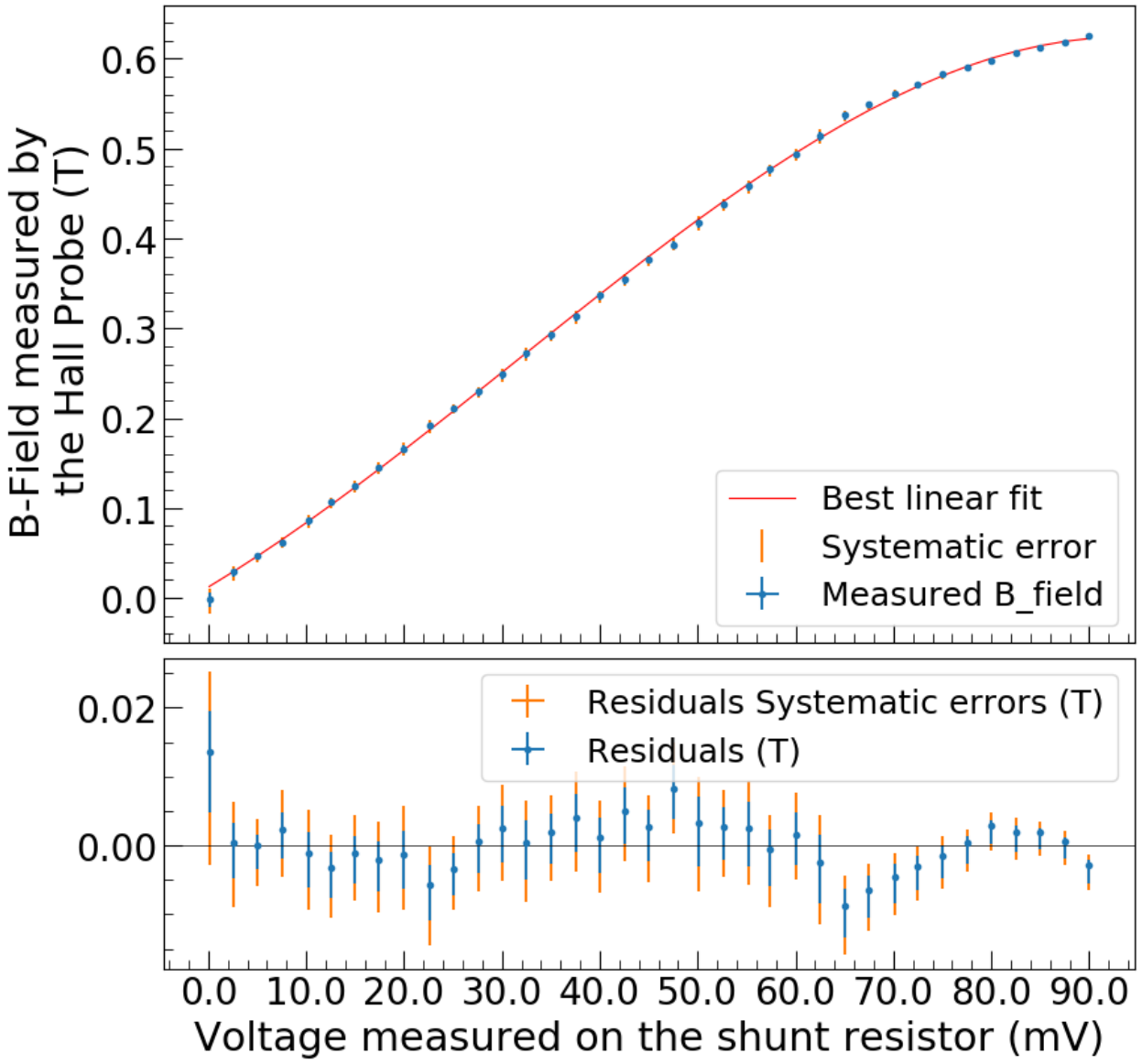

Figure 2: Calibration of the power supply to determine the magnetic field produced by the electromagnets for a certain voltage read on the shunt resistance of the power supply. The least-square polynomial fit of third degree shown gives a reduced chi squared of 1.02 and the residuals are shown below the fit. The systematic error on the B-field at each data point comes from the systematic 1 mV uncertainty when placing the probe in the middle of the magnets. The magnitude of the field gets saturated at higher voltages.

3.2 Results and Error analysis

The error on the polynomial fit is derived from a least-square fit for which each data point had an error of $0.003 * V + 0.1$ mV associated to the voltmeter precision where V is the measured voltage on the hall probe in mV [6]. During the interpolation step, the error on

the interpolated point is based on the standard variation [7] and is found by multiplying the distance to the nearest data point by the gradient of the fit at that nearest data point. The error on the polynomial fit is computed via a classical polynomial regression error analysis for a 3^{rd} degree polynomial and yields best fit parameters of a=$(-7.5 \pm 0.3) \times 10^{-7}$, b=$(7.1 \pm 0.6) \times 10^{-5}$, b=$(6.5 \pm 0.2) \times 10^{-3}$ and d=$(1.2 \pm 0.3) \times 10^{-2}$ where the expression for the fit of the magnetic field is given by

$$B = a * V^3 + b * V^2 + c * V + d$$

where this time, V is the voltage measured across the shunt resistor.

A systematic error analysis is also perform, as shown in figure 2 in order to account for the fact that the cadmium lamp used in further experiments is placed 'in the middle' of the magnet by eye. Hence, numerous readings of the voltage across the Hall probe are taken while placing the probe in the middle of the magnets by eye (without looking at the voltmeter as for the calibration setting). Computing the standard deviation of these measurements gives an estimate for the systematic error uncertainty of 1 mV associated with the magnetic field value used in subsequent experiments.

Including all the data and error analysis above, the reduced chi squared of the polynomial fit is of 1.02. The residuals of the fit shown in figure 2 are roughly randomly distributed, which means the fit is reliable and that the calibration can be used with confidence for further experimentation.

4 Fabry-Pérot Measurement

4.1 Theory

The FP apparatus produces interference patterns, such as the one shown in figure 1b. The observed rings can therefore be analyzed to obtain their respective radii. As we apply a magnetic field of magnitude B to the Cadmium lamp, these rings will split into three, as Cadmium atoms will undergo Zeeman splitting as a function of their quantum number m_l. The ring of order n corresponding to atoms with a 0 magnetic quantum number, $r_{n,b}$, will

then be in between the two other rings, one with a smaller radius which we will call $r_{n,a}$, and one with a larger radius which we will call $r_{n,c}$.

The wave number difference between two spectral lines, $\Delta\bar{v}$, can then be computed using the Zeeman effect. Indeed, if we let t be the thickness of the FP lens, $\Delta\bar{v} = \frac{\delta}{2t\Delta}$, where δ is given by

$$\delta = \frac{1}{n}\sum_{i=1}^{n}(r_{i,b}^2 - r_{i,a}^2) = \frac{1}{n}\sum_{i=1}^{n}(r_{i,c}^2 - r_{i,b}^2), \tag{3}$$

where n corresponds to the number of rings where splitting is observed, and Δ is given by

$$\Delta = \frac{2}{n}\sum_{i=1}^{n}(r_{i,c}^2 - r_{i-1,c}^2 + r_{i,a}^2 - r_{i-1,a}^2). \tag{4}$$

[2]

In fact, δ represents the mean difference in squared radius between a ray of quantum component $m_l = 0$ and one of component $m_l = \pm 1$. This means δ should be the same when using the outer ring or the inner ring. In a similar manner, Δ represents the mean of the difference of radius squared between rings of adjacent order. The derivation of the Bohr magneton using the FP apparatus is then given by:

$$\mu_B = \frac{hc\Delta\bar{v}}{2B}, \tag{5}$$

where $h = 6.62607015 \times 10^{-34}$Js is Planck's constant and $c = 299792458$m/s is the speed of light. Both quantities are considered to be exact [8] [2].

4.2 Results

Figure 3a shows the picture of a diffraction pattern taken at 0.62 ± 0.06 T, with the fitted centre and line profiles passing through the centre both in the x and y axes. We see that the line profile in y shows the peaks of the pattern more clearly than the one in x, especially in the region between 300 and 1300 pixels. Figure 1b shows a fit of multiple gaussians to extract the location of the peaks in that region. More information on how the fit is performed can be found in section 4.3. From the gaussian fit, we can extract the position of the different peaks

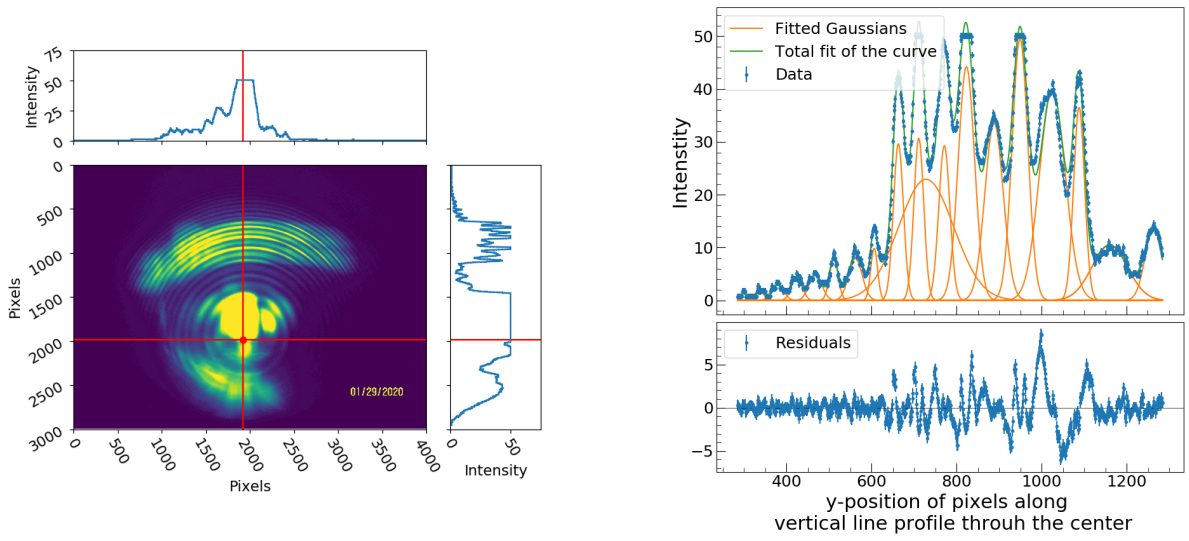

(a) (b)

Figure 3: Analyzed diffraction pattern for a picture took at a magnetic field value of 0.62±0.06 T without the polarizing filter. **(a)** The pattern is shown with the red dot being our estimate for the centre ($x = 1926 \pm 71$ pixels, $y = 1985 \pm 33$ pixels) and the red lines being the vertical and horizontal line profiles that are subsequently analyzed. The reduced Chi squared of the centre fit is 9.71. On each side of the figure, the pixel intensity profile along each red line is shown. In these intensity plots, we capped the intensity to be able to see the fluctuations all the way along the line (otherwise we only see the central bright spot) Note that the light source creates a big noisy bright region in our data. **(b)** Multiple gaussian fit of the vertical line profile presented in figure 3a. The gaussian peaks are fitted on top of a larger gaussian function which gets rid of the underlying intensity where we find the peaks (when the fit is performed, it makes them more flat). The error on each intensity value is of 0.6 (see section 4.3 for derivation). The residuals are shown below the graph and appear to be well-behaved. The little remaining structure in the residuals is due to the underlying larger gaussian fit but is not worrying since the error on the peaks' locations is dominated by the error on the centre.

and compute their distance from the centre. In order to identify the quantum component of each ring, we use the polarizer and analyze different images, letting either the $m_l = 0$ or the $m_l = \pm 1$ spectral rings through. Table 1 shows the values of the radii squared as well as the value of δ and Δ. Using the values computed in the table, we find that, using the average of the splits δ_{ab} and δ_{bc}, the value of the Bohr magneton at 0.62 ± 0.06 T is given by $(7 \pm 6) \times 10^{-24}$ J/T.

Doing a similar analysis for pictures taken at a magnetic field of 0.50 ± 0.03 T gave

Ring Order	1	Δ_{12}	2	Δ_{23}	3	Δ_{34}	4
R_a^2	5.24×10^5	4.03×10^5	9.27×10^5	4.25×10^5	1.352×10^6	3.99×10^5	1.751×10^6
δ_{ab}	1.32×10^5		1.49×10^5		1.24×10^5		1.53×10^5
R_b^2	6.55×10^5	4.20×10^5	1.076×10^6	4.00×10^5	1.476×10^6	4.28×10^5	1.904×10^6
δ_{bc}	1.51×10^5		1.28×10^5		1.51×10^5		1.23×10^5
R_c^2	8.07×10^5	3.97×10^5	1.204×10^6	4.22×10^5	1.626×10^6	4.01×10^5	2.027×10^6

Table 1: Radii squared of the rings in pixels squared found and values of the splitting for a magnetic field of 0.62 ± 0.06 T. Value of the radii are found by taking the average of the positions of the peaks on two different pictures taken at the same fields. The error is vastly dominated by the error on the centre of the fit, which is of 0.02×10^5 pixels^2. We find that $\delta_{ab} = (1.38 \pm 0.40) \times 10^5$ and $\delta_{bc} = (1.36 \pm 0.40) \times 10^5$ while $\Delta = (4.1 \pm 0.5) \times 10^5$, where the errors come from the standard deviation of the values. Note that in this table, the ring order starts at 1 for simplicity even if the first line does not really correspond to the first ring. However, this does not change the results since the ring order has no influence in the formula of the Bohr magneton in equation 5.

the same result. We therefore conclude that our final value for the Bohr magneton is of $(7 \pm 6) \times 10^{-24}$ J/T. Furthermore, the systematic on the magnetic field does not change the final uncertainty on the results, as it is negligible compare to the error on the centre of the pattern.

4.3 Data analysis

In order to analyze the diffraction patterns, we proceed in two steps. First, we perform a cross-correlation with a circular pattern model to estimate the location of the centre of all rings. We then plot the pixel intensity captured by the camera along the vertical line and the horizontal line passing through this point as shown in figure 3a. We then determine the radii of the rings by computing the distance between our best estimate of the centre and the light intensity peaks.

On the first hand, as the rings are not guaranteed to be concentric, we use a method of cross correlation to find the best possible location on one image for the centre of all rings. We perform a convolution with a circular ring model in Fourier space using the Fast Fourier Transform method. By repeating this technique multiple times with varying initial guesses for the radii of the circles, we are then able to derive an error estimate on the centre of the diffraction pattern.

On the other hand, once the centre is found in the images, we fit Gaussian functions to each light intensity peak in the vertical line profile (see section 4.2) passing through the centre. We first apply a Gaussian filter to the data to reduce the noise around the peaks. This allows us to perform initial Gaussian fits on the filtered data to obtain proper guesses on the peaks' locations. We then use these guesses to fit Gaussian functions on the unfiltered data, and the radii of the rings are then given by calculating the distance between the centre found above and the peaks' locations obtained from the raw data fits. Random error estimate for the peak locations comes from taking multiple pictures of interference patterns for unchanged set-ups (i.e., by keeping constant the power supply output, the interference pattern resolution , and the camera settings). We then use the change in location of the light intensity peaks from one image to the other to calculate the error in our measurements as a standard deviation. The total random error found on the radii of the circles is then given by the combination of the error found on the light intensity peaks locations and the error on the centre of the interference pattern. As it has been noted earlier, it turns out the the error is dominated by the error on the centre.

For the FP experiment, the systematic uncertainty comes from the pixel sensitivity of the CCD camera. To properly estimate this error, we take multiple pictures of the same image to obtain an average difference in intensity for each pixel. Then, assuming all pixels have uniform sensitivity, we compute the mean difference for all pixels, which we use as our error estimate. This gives an uncertainty of 0.6 in pixel intensity units at each pixel.

Combined together, the errors mentioned above provide the error on the calculated rings radii. We then have all the necessary elements to perform an error propagation calculation on the Bohr magneton, which is given as follows :

$$\sigma^2_{\mu_B} = \frac{h^2c^2\delta^2}{16t^2B^4\Delta^2}\sigma^2_B + \frac{h^2c^2}{16t^2B^2\Delta^2}\sigma^2_\delta + \frac{h^2c^2\delta^2}{16t^2B^2\Delta^4}\sigma^2_\Delta. \tag{6}$$

We give the error propagation calculation for δ and Δ in 7.1.

4.4 Validity

The final result obtained for the Bohr magneton is of $(7 \pm 6) \times 10^{-24}$ J/T. Comparing our result to the accepted value of $9.2740100783(28) \times 10^{-24} J/T$ [1], we see there is a clear accordance between our experimental value and the accepted one. This is in part due to the fact the error on our result is almost as great as the result itself. This is probably caused by the noisy bright spot created by the light source in our images (see figure 3a). This is the reason why the uncertainty on the centre of the images is so big and drives our overall error up. Furthermore, one could compute the index of refraction of the air in the lab to correct for the error arising in taking the value in vacuum.

5 Conclusion

To summarize, during this experiment, the Zeeman effect was used in order to observe the splitting of light rays emitted by a Cadmium lamp and measure the value of the Bohr magneton. After having successfully calibrated the electromagnets, a thorough analysis of diffraction pattern images using cross correlation and least square fittings was achieved, allowing us to validate the Zeeman effect and the value of the Bohr magneton 4.4. The next steps for this experiment would be to effectively model the noise created by the source in our images. Indeed, the fact that the light source appears in our images makes the centre fit hard, as discussed above. If we had a reliable model for this light source effect on our images, we could subtract it to our data and get much clearer diffraction patterns and subsequently much more precise estimates on the centre of the rings. This way, it would be possible to get a more precise result for the Bohr magneton. A laser could also be used to aligned the optical elements in order to obtain a better definition on the images, which would help improve the fit.

6 Aknowledgments

We would like to thank professor Jonathan Sievers for his help with the cross correlation method and the associated error analysis.

References

[1] NIST, "Fundamental Physics Constants." [Online]. Available: https://physics.nist.gov/cgi-bin/cuu/Value?mub 1, 10

[2] A. Melissinos, "Experiments in Modern Physics (First Ed.)," 1996. [Online]. Available: http://sky.campus.mcgill.ca/Exp/exp.a5w# 1, 6

[3] "Observing the normal Zeeman effect in transverse and longitudinal configuration Spectroscopy with a Fabry-Perot etalon." [Online]. Available: https://people.stfx.ca/cadams/physics475/labs/zeeman/QueenMaryUnivLondon_Zeemaneffect.pdf 1

[4] S. C. McGill, "Hall Probe EQ3485," 2014. [Online]. Available: http://293-pc0304.campus.mcgill.ca/equip/manuals/eq0590.pdf 3

[5] P. D. Stoltenberg, J. and R. Van Dyck, "Zeeman Effect in Mercury," Feb. 2007. [Online]. Available: http://courses.washington.edu/phys432/zeeman/zeeman_effect.pdf 3

[6] Fluke, "Fluke 77 Users Manual," Feb. 2018. [Online]. Available: https://dam-assets.fluke.com/s3fs-public/77_____umeng0200.pdf 4

[7] K. Gullikson, "Interpolation with error propagation," Jul. 2015. [Online]. Available: https://gist.github.com/kgullikson88/147f6beb6256307d1360 5

[8] BIPM, "Resolutions of the 26th GCPM," Nov. 2018. [Online]. Available: https://www.bipm.org/utils/common/pdf/CGPM-2018/26th-CGPM-Resolutions.pdf 6

7 Appendix

7.1 Error propagation for δ and Δ

δ and Δ both are parameters depending only on the radii of rings. We therefore only need to propagate the error on the radii to obtain the error on δ and Δ. Hence,

$$\sigma_\delta^2 = \frac{1}{n^2}\sum_{i=1}^{n} 4(r_{i,b}^2\sigma_{r_{i,b}}^2 + r_{i,a}^2\sigma_{r_{i,a}}^2) = \frac{1}{n^2}\sum_{i=1}^{n} 4(r_{i,c}^2\sigma_{r_{i,c}}^2 + r_{i,b}^2\sigma_{r_{i,b}}^2), \tag{7}$$

and

$$\sigma_\Delta^2 = \frac{4}{n^2}\sum_{i=1}^{n} 4(r_{i,c}^2\sigma_{r_{i,c}}^2 + r_{i-1,c}^2\sigma_{r_{i-1,c}}^2 + r_{i,a}^2\sigma_{r_{i,a}}^2 + r_{i-1,a}^2\sigma_{r_{i-1,a}}^2) \tag{8}$$